International Journal of Biometeorology
https://doi.org/10.1007/s00484-024-02771-w

ORIGINAL PAPER

Monitoring anomalies on large-scale energy and water balance components by coupling remote sensing parameters and gridded weather data

Antonio Teixeira[1] · Janice Leivas[1,2] · Celina Takemura[1,2] · Edlene Garçon[1,2] · Inajá Sousa[1] · Ana Azevedo[1]

Received: 3 April 2024 / Revised: 21 August 2024 / Accepted: 26 August 2024

Abstract
The SAFER (Simple Algorithm for Evapotranspiration Retrieving) algorithm was applied with MODIS images and gridded weather data from 2007 to 2021, to monitor the energy balance components and their anomalies, in the Atlantic Forest (AF) and Caatinga (CT) biomes inside the coastal agricultural growing zone, Northeast Brazil. Considering the long-term data, the R_n values between the biomes are not significantly different, however presenting distinct R_n partitions into latent (λE), sensible (H), and ground (G) heat fluxes between biomes. The R_n values annual averages are 9.40 ± 0.21 and 9.50 ± 0.23 MJ m^{-2} d^{-1}, for AF and CT, respectively. However, for respectively AF and CT, they are respectively 5.10 ± 1.14 MJ m^{-2} d^{-1} and 4.00 ± 0.99 MJ m^{-2} d^{-1} for λE; 3.80 ± 1.12 MJ m^{-2} d^{-1} and 5.00 ± 1.00 MJ m^{-2} d^{-1} for H; 0.50 ± 0.12 MJ m^{-2} d^{-1} and 0.40 ± 0.10 MJ m^{-2} d^{-1} for G, yielding respective mean evaporative fraction ($Ef = \lambda E/(R_n - G)$ values of 0.60 ± 0.12 and 0.50 ± 0.15. Anomalies on λE, H, and Ef were detected through standardized index for these energy balance components by comparing the results for the years 2018 to 2021 with the long-term values from 2007 to each of these years, showing that the energy fluxes between surfaces and the lower atmosphere, and then the root-zone moisture conditions for both biomes, may strongly vary along seasons and years, with alternate positive and negative anomalies. These assessments are important for water policies as they can picture suitable periods and places for rainfed agriculture as well as the irrigation needs in irrigated agriculture, allowing rational agricultural environmental management while minimizing water competitions among other water users, under climate and land-use changes conditions.

Keywords Net radiation · Evaporative fraction · Standardized index · Environmental management · Atlantic Forest · Caatinga

Introduction

Climate and land-use changes, affecting the energy and water balance components, have been detected worldwide, making geotechnologies powerful tools for monitoring these components, to subsidize policies for rational environmental management (Jardim et al. 2022; Rampazo et al. 2020; Safre et al. 2022; Teixeira et al. 2017a, b; 2021a). Understanding the effects of these changes is critical for ecological restoration (Yang et al. 2016; Zhang and Zhang 2019), demanding large-scale studies to support sustainable explorations of the natural resources (Almeida et al. 2023; Araujo et al. 2019; Santos et al. 2020). These tools on different temporal and spatial scales, can be also used to detect anomalies on the energy and water balance components for specific periods, by using long-term satellite images and weather data (Beguería et al. 2014; Bento et al. 2018; Gouveia et al. 2017; Vicente-Serrano et al. 2018; Yang et al. 2014; Zhang et al. 2019, 2021).

Accounting the energy balance components, the net radiation (R_n) is the difference between incoming and outgoing energy fluxes of both short and long wavelengths, being partitioned into latent (λE), sensible (H), and ground (G) heat fluxes, and the magnitudes of these partitions are dependent on solar radiation levels and the root-zone moisture conditions. Monitoring λE is outstanding, because it represents the energy used for evapotranspiration, which is the main water use from any agroecosystems. On one hand, although evapotranspiration is related to agricultural

✉ Antonio Teixeira
heribertoteixeira11@gmail.com

[1] Federal University of Sergipe: Universidade Federal de Sergipe, São Cristóvão, Brazil

[2] Embrapa Territory, Embrapa, Campinas, Brazil

production, increases of its rates means less water availability for other water sectors (Teixeira et al. 2023). On the other hand, the magnitude of H may indicate warming or cooling conditions (Bhattarai et al. 2017; Teixeira et al. 2017a, b; 2021a; Zhang et al. 2016). Teixeira et al. (2017b) showed that the replacement of natural vegetation by sugarcane, in Southeast Brazil, reduced λE, increasing H, while when this replacement happened with coffee, the opposite situation was verified, increasing λE, dropping H. Quantifying these components, describing their dynamics and anomalies along the years, is meaningful to assess the dimension of environmental impacts (Yang et al. 2016; Zhang and Zhang 2019; Zhang et al. 2021).

The Normalized Differences Vegetation Index (NDVI) is worldwide used to indicate vegetation greenness (Bento et al. 2018; Brouwers et al. 2015). The NDVI standardized index was developed by Peters et al. (2002), to describe the probability of variation from its normal value over multiple years of data on a weekly time step. However, in terms of reflecting impacts of environmental stress on vegetation, NDVI often shows delayed, regarding the root-zone moisture responses (Zhang et al. 2019). Thus, standardized indices, to detect environmental anomalies, have been generally based on large-scale NDVI, precipitation (P), actual evapotranspiration (ET), and soil moisture (Hao and AghaKouchak 2013; Kim and Rhee 2016; Mu et al. 2011; Teixeira et al. 2021b, Vicente-Serrano et al. 2018; Yao et al. 2010; Zhang et al. 2021), such as Standardized Soil Moisture Index (SSI) (Hao and AghaKouchak 2013); the Standardized Precipitation Evapotranspiration Index (SPEI) (Vicente-Serrano et al. 2018; and the Standardized Moisture Anomaly Index (SZI) (Zhang et al. 2021). The inclusion of the energy balance components in these assessments is important for environmental monitoring, as they are highly variable on both space and time (Ford and Labosier 2017; Otkin et al. 2013; Teixeira et al. 2017a, b, 2021a, b; Zhang and Zhang 2019; Zhang et al. 2021.

According to Vicente-Serrano et al. (2018), ET anomaly analyses in semi-arid regions are appropriate, as there are more instabilities on the root-zone moisture levels, affecting biomass production and canopy structure (Zhang et al. 2016). Zhang et al. (2015) developed a water moisture index, by incorporating some advantages regarding other indices, whose performance has been verified on different scales for long-term water assessments. Their index employs a water-energy balance model to estimate the aggregate moisture departure. Hence, an accurate assessment of environmental impacts on vegetation activity is crucial for understanding the response of the biomes to anomalies (Zhang et al. 2019, 2021), especially under water scarcity conditions, as in case of some Northeast Brazilian areas.

In the coastal Brazilian biomes, inside the Northeast region, the ecosystems are experiencing environmental impacts because of deforestations; burnings; air, water and soil pollutions, as well intensive agricultural crops replacing the natural vegetation (Lewinsohn and Prado 2005; Mariano et al. 2018). This is the case of SEALBA, acronym for the agricultural growing region involving the states of Sergipe (SE), Alagoas (AL) and Bahia (BA), with increasing mixed agroecosystems within the Atlantic Forest (AF) and Caatinga (CT) biomes, over the last years, and these land use changes, together climate instabilities, affect the available energy partitions into λE and H, what can increase water consumptions or warming conditions. The delimitation of the agricultural potential for SEALBA was based on the average totals of precipitation ranging between 450 and 1400 mm, from April to September. According to Procopio et al. (2019), these rainfall amounts could supply water for several crops (grains, fruits, sugar cane, forestry, and pasture). However, to know the real water availabilities for agriculture, besides rainfall as input, the output, i.e., water fluxes represented here by λE in energy units, must be also considered. In the SEALBA coastline, is the AF biome and more to the west side is the CT biome, both experiencing replacements of their natural vegetation by crops. Despite their aptitude for agriculture when water is available, this fast replacement, together with climate changes, may increase environmental impacts. The use of long-term energy balance data and standardized indices based on its components is suitable for policy decision-making under these unstable conditions.

Some field energy and water balance studies were done by different methods in the Brazilian AF and CT biomes (Marques et al. 2020; Pereira et al. 2010; da Silva et al. 2017; Teixeira et al. 2008). However, time specific point measurements are not suitable for large-scale long-term accountings, because of strong spatial and temporal variations on the energy and mass exchanges between surfaces and the lower atmosphere. Few efforts have been carried out for monitoring the energy and water balance components along the years inside these biomes considering a large data series for average conditions, allowing to monitor anomalies for specific periods. These analyzes can help to understand the responses of natural vegetation and agricultural crops to the environmental impacts.

Remote sensing from satellites, together with weather data from field stations, have been used for energy and water balance assessments through algorithm applications in distinct agroecosystems at different spatial and temporal scales (Allen et al. 2007; Bastiaansssen et al. 1998; Teixeira 2010). These algorithms are very useful to evaluate the impacts from human activities upon natural resources, due to their efficiencies to account these components at different spatial and temporal resolutions. Because of its operationality, the Penman–Monteith (PM) equation has been inserted in some of remote-sensing algorithms (Cleugh et al. 2007; Consoli and Vanella 2014; Consoli et al. 2016;

Nagler et al. 2013; Olivera-Guerra et al. 2018), which when applied with gridded weather data, are suitable for using with low spatial resolution satellite images, but with good temporal resolutions (Mateos et al. 2013; Teixeira et al. 2023; Vanella et al. 2019), as for example, applying to MODIS images with spatial resolution of 250 m and 1,000 m in the visible and thermal bands, respectively, at daily temporal resolution (Teixeira et al. 2013).

Considering operational aspects of the Penman–Monteith equation, the SAFER (Simple Algorithm for Evapotranspiration Retrieving) algorithm was developed by using simultaneous field and remote sensing measurements in Northeast Brazil to estimate the energy and water balance components. The bands 1 to 7 from Landsat 5 satellite; and bands 1–2 together with the bands 31–32 from MODIS sensor were used together with micrometeorological data to derive and validate all the SAFER´s equations (Teixeira et al. 2008, 2010; 2013). The reason for the SAFER´s choice in the current research, besides its applicability, other important advantage, regarding other algorithms, is that in its newer version there is no need of the thermal bands, being possible to use only the red (MODIS spectral range 0.62–0.67 µm) and near infrared bands (MODIS spectral range 0.84–0.87 µm), more easily available (Consoli and Vanella 2014). In addition, the thermal bands of the MODIS sensor, having a spatial resolution of 1 km, means that the images should cover more mixed surface types, when comparing with the 250-m spatial resolution of its red and near infrared bands.

Aiming to implement an operational monitoring system for biomes experiencing climate and land-use changes, taking the SEALBA region as a reference, we tested the latest version of the SAFER algorithm, by using MODIS MOD13Q1 reflectance products and long-term weather data from 2007 to 2021 at the same satellite 16-day timescales, to retrieve the dynamic of the energy and water balance conditions along the years. Besides characterizing average conditions, we used a standardized index based on the energy balance components (EB_{STD}) for further anomaly assessments on these components for specific periods of the four last years of this long-term data set. The authors believe that the success of applications for this specific region may encourage replications of the methods in other environmental conditions with simple calibrations of the modelling equations.

Material and methods

Biomes and data set

Figure 1 shows the location of the SEALBA agricultural growing region within the Brazilian states of Sergipe – SE, Alagoas – AL, and Bahia- BA, in Northeast Brazil (Fig. 1a); biomes involved by the region (Fig. 1b) according to the Geographic and Statistical Brazilian Institute (IBGE - www.ibge.gov.br); and altitudes together with the 17 weather stations used (Fig. 1c) from the National Meteorological Institute (INMET - https://www.gov.br/agricultura/pt-br/assuntos/inmet).

Considering the MODIS pixel size of 250 m, the SEALBA region comprises 6.2 Mha (Fig. 1a), involving the Atlantic Forest (AF) and Caatinga (CT) biomes (Fig. 1b). The AF areas, mostly below 275 m of altitude, are in a portion closer to the coastline, while CT areas are located more to the west side, being the majority above 275 m of altitude (Fig. 1b and c).

The AF biome is characterized by forest vegetation, involving dense and open rain forests, semi-decidual season forests. The climate is tropical humid but with mixed microclimates involving natural and anthropized areas (Ribeiro et al. 2009). The CT biome has species composed by trees and shrubs with characteristics that allow environmental adaptations, under high air temperatures but at low air humidity levels (Santos et al. 2014). Both biomes within SEALBA have been experiencing fast replacement of their natural vegetation by crops.

The input weather data for the large-scale energy balance modelling were incident global solar radiation (R_G); air temperature (T_a), air relative humidity (RH), and wind speed (u); for the calculation of reference evapotranspiration (ET_0) (Allen et al. 1998) and the latent heat fluxes – λE, applying the SAFER algorithm (Teixeira et al. 2017a, b, 2021a, b). Through a geographic information system (GIS), these data were interpolated using the geostatistical "moving average" method and layered with the remote sensing parameters, contributing to a better spatial characterization of the energy balance components at the spatial resolution of the MODIS images.

The bands 1 (red) and 2 (infrared) from the MODIS sensor (MOD13Q1 reflectance product) were downloaded from the site of EARTHDATA Aρρ EEARS (https://lpdaacsvc.cr.usgs.gov/appeears/) and used together with the weather data from the stations of INMET. The images have spatial and temporal resolutions of 250 m and 16 days, respectively, giving 23 free-cloud images in a year. The MOD13Q1 product provides the NDVI and the Enhanced Vegetation Index (EVI). The algorithm chooses the best available pixel value from all the acquisitions from the 16-day period. The criteria used is low clouds, low view angle, and the highest NDVI/EVI value. Along with these vegetation layers, the HDF file has reflectance bands 1 and 2, used in the current research.

Considering the long-term period from 2007 to 2021, it was possible to quantify anomalies for specific periods from 2018 to 2021, in the AF and CT biomes within the SEALBA agricultural growing. To retrieve the energy and water balance components from all MODIS images and

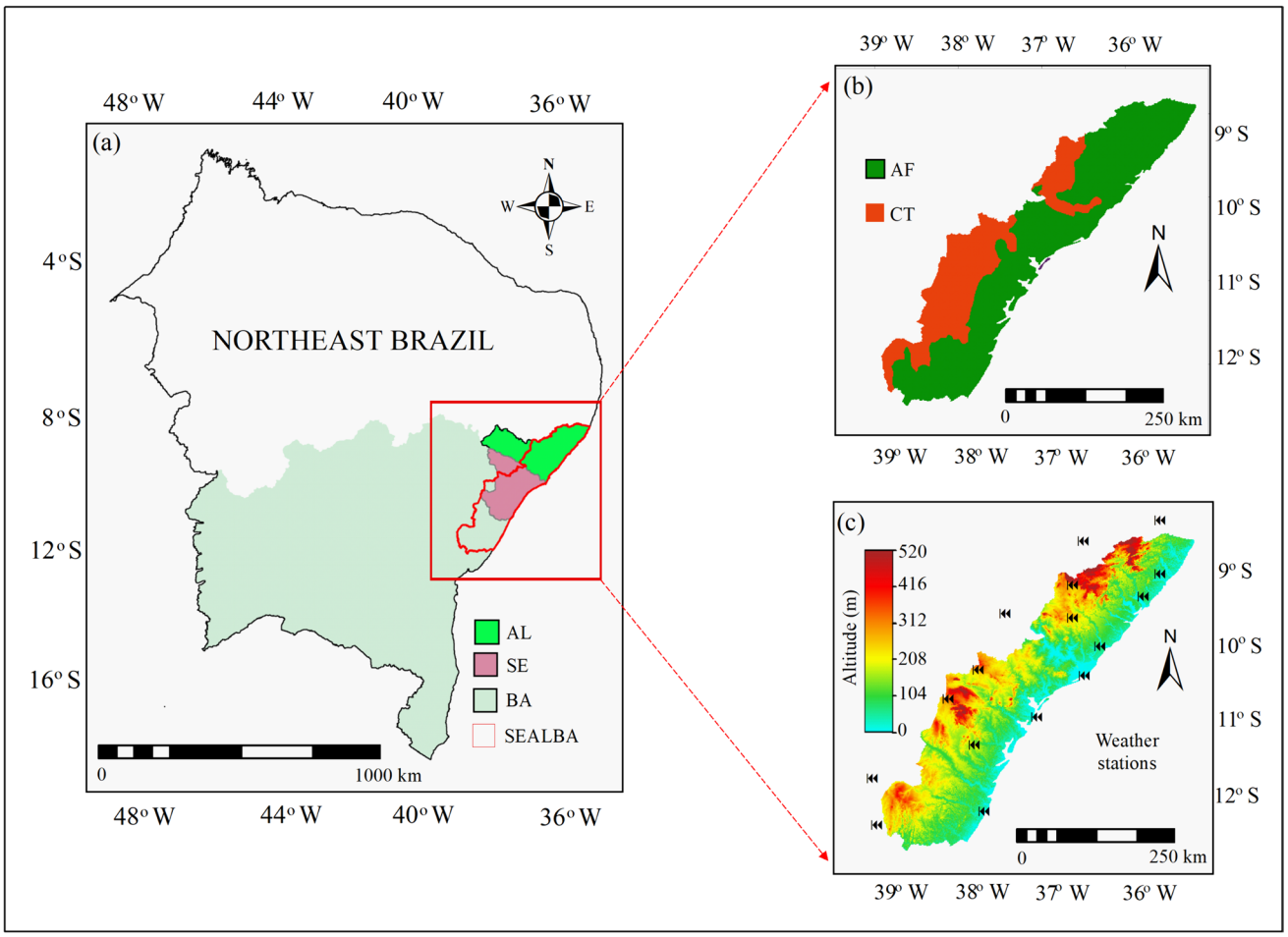

Fig. 1 Location of the SEALBA agricultural growing region in Northeast Brazil, involving the states of Sergipe—SE, Alagoas—AL, and Bahia – BA (**a**); the biomes within the region (**b**); and altitudes together with the weather stations (**c**)

gridded weather data, the SAFER's equations were applied by using a script built in the Integrated Land and Water Information System (ILWIS), version 3.8.6, which is a geographic information system (GIS) and remote sensing software for both vector and raster processing (https://52north.org/news/new-ilwis-3-8-6-release/).

Large-scale energy balance modelling

Calculations of Normalized difference vegetation index (NDVI) and surface albedo (α_0)

After clipping the MODIS reflectance images for the SEALBA region, the Normalized Difference Vegetation Index (NDVI) was calculated and incorporated in the modelling steps as a surface cover and root-zone moisture remote-sensing indicator:

$$NDVI = \frac{\rho_2 - \rho_1}{\rho_2 + \rho_1} \quad (1)$$

where ρ_1 e ρ_2 are respectively the MODIS reflectance from bands 1 (red) and 2 (near infra-red).

The pixel values of surface albedo (α_0) were acquired as:

$$\alpha_0 = a + b\rho_1 + c\rho_2 \quad (2)$$

where a, b, and c are regression coefficients, which in the Northeast of Brazil, were 0.08, 0.41, and 0.14, from simultaneous remote sensing and field measurements, involving distinct irrigated crops and natural vegetation, under strong contrasting hydrological conditions (Teixeira 2010; Teixeira et al. 2013).

Estimation of surface temperature (T_0)

For estimation of the daily surface temperature (T_0) pixel values, without the MODIS thermal bands, this was done

considering the short and long-wave radiation balance components. The remote sensing parameters and weather data were combined, through the Stefan-Boltzmann principle for the emitted both atmosphere and surface radiations (Silva et al. 2019):

$$T_0 = \frac{\sqrt[4]{R_G\left(1-\alpha_0\right)+\sigma\varepsilon_A T_a^4 - R_n}}{\sigma\varepsilon_0} \tag{3}$$

where ε_A is the atmospheric emissivity, ε_0 is the surface emissivity, and $\sigma = 5.67\ 10^{-8}$ W m^{-2} K^{-4} is the Stefan-Boltzmann constant.

R_n was estimated through the Slob equation (Almeida et al. 2023):

$$R_n = \left(1-\alpha_0\right)R_G - a_L\tau_{sw} \tag{4}$$

where τ_{sw} is the short-wave atmospheric transmissivity calculated as the ratio of R_G to the incident solar radiation at the top of the atmosphere (R_{TOP}) calculated by astronomic parameters, and a_L is a regression coefficient up scaled through T_a pixel values.

$$a_L = a_T T_a + b_T \tag{5}$$

being a_T and b_T for the Northeast Brazil were found as 6.8 and -40, respectively (Teixeira 2010).

The ε_A and ε_0 values were calculated according to Safre et al. (2022):

$$\varepsilon_A = a_A\left(\ln\tau_{sw}\right)^{b_A} \tag{6}$$

$$\varepsilon_0 = a_0 \ln NDVI + b_0 \tag{7}$$

where a_A, b_A, a_0, and b_0 are regression coefficients, which were reported as 0.94, 0.11, 0.06, and 1.00, respectively, for the Northeast Brazil (Teixeira 2010; Teixeira et al. 2013).

Net radiation partition

To estimate the λE, the ratio of the actual (ET) to reference (ET_0) evapotranspiration (ET_0), was first modeled for the satellite overpass time:

$$\left(\frac{ET}{ET_0}\right)_{sat} = \exp\left[a_{sf} + b_{sf}\left(\frac{T_0}{\alpha_0 NDVI}\right)\right] \tag{8}$$

where the regression coefficients a_{sf} and b_{sf} found for the Brazilian Northeast were 1.90 and -0.008 (Venâncio et al. 2021).

Equation 8 does not work for water bodies or mixture of land and water (NDVI < 0); thus, the concept of equilibrium evapotranspiration (Raupasch 2006) is introduced in the SAFER algorithm for pixels under these conditions, with the equilibrium latent heat fluxes (λE_{eq}), at daily timescale, considered as:

$$\lambda E_{eq} = \left(\frac{\Delta\left(R_n - G\right)}{\Delta+\gamma}\right) \tag{9}$$

where Δ is the inclination of the curve relating the saturation vapor pressure (e_s) and T_a, γ is the psychrometric constant, and G is estimated according to Teixeira (2010):

$$G = \left[a_G \exp\left(b_G\alpha_0\right)\right]R_n \tag{10}$$

being a_G and b_G regression coefficients, found to be 3.98 and -25.47, respectively, for the Northeast Brazil.

Considering that the satellite overpass values of the ET/ET_0 fraction does not differ so much from the daily ones (Teixeira 2010), throughout conditional functions applied to the NDVI values, the daily λE pixel values were estimated considering the daily averages of the reference evapotranspiration for this timescale ($ET_{0_{24}}$):

$$\lambda E = 2.45\left(\frac{ET}{ET_0}\right)_{sat} ET_{0_{24}} or \lambda E_{eq} \tag{11}$$

being $ET_{0_{24}}$ calculated by using the gridded daily weather data on R_G, T_a, RH, and u (Allen et al. 1998) and 2.45 a unit conversion factor.

To close the simplified energy balance equation, H was estimated as a residue, having retrieved all the other energy balance components (Teixeira et al. 2017a, 2021a):

$$H = R_n - \lambda E - G \tag{12}$$

To infer the root-zone moisture conditions, the evaporative fraction (Ef) was estimated as:

$$Ef = \frac{\lambda E}{R_n - G} \tag{13}$$

Standardized index for the energy balance components

Following Teixeira et al. (2021b), Zhang et al. (2019), and Zhang et al. (2021), to detect anomalies on the energy balance components, regarding the 16-day periods of the MODIS MOD13Q1 product and for the year, the following equation was tested to calculate the standardized index (STD) for the energy balance (EB) components from 2018 to 2021:

$$EB_{STD} = \frac{EB - EB_{mean}}{EB_{SD}} \tag{14}$$

where EB_{STD} is the standardized index for λE, H or Ef for the period (16-day or year timescales, from 2018 to 2021); EB are their values for the specific year (2018, 2019, 2020,

and 2021); EB_{mean} are their long-term averages (2007–2018, 2007–2019, 2007–2020, and 2007–2021); and EB_{SD} are the pixel-by-pixel standard deviations (2007–2018, 2007–2019, 2007–2020, and 2007–2021).

Results

Main weather drivers

As for the energy balance partitions the main weather drivers are precipitation (P) and incident global solar radiation (R_G), Fig. 2 shows their average pixel values regarding the long-term period from 2007 to 2021, and standard deviations (SD), for AF and CT within SEALBA, at the MOD13Q1 reflectance 16-day timescale, in terms of Day of the Year (DOY).

From Fig. 2a, it is noticed that rainfalls are concentrated in the middle of the year for both biomes, AF and CT, with the high amounts for AF. The highest P pixel values occur from April to July (DOY 097–208), when the MODIS 16-day average totals are above 60 mm for AF, and higher than 50 mm for CT. The lowest rainfall amounts, with P mean totals below 15 mm in both biomes at this timescale, are from November to January (DOY 305–016), which limit λE, increasing H. Regarding the annual scale, the mean total in CT, accounting 780 mm yr^{-1}, is 83% of that for AF (936 mm yr^{-1}). The largest spatial variations between biomes are for AF, where the SD values represent 17% of the annual P, while for CT the corresponding percentage is 14%.

As shown in Fig. 2b, the R_G average values have an inverse tendency along the year, when compared with those for P. The highest R_G levels are from October to March (DOY 289–065), with averages above 21.0 MJ m^{-2} d^{-1} for both biomes, which together with lower rainfall amounts are in favor for warmer conditions. The lowest R_G rates happen at the middle of the year in June (DOY 161–176), when the average drops to below 14.5 MJ m^{-2} d^{-1} but under the highest rainfall amounts. Much lower differences on R_G values arise between AF and CT when comparing with P, being the average R_G for AF 99% of that for CT. Similar R_G spatial variations between biomes are detected in the middle of the year, when SD accounts only for 3% of the average pixel values, but the highest SD occur in AF outside this moistiest period, mainly at the start of the year, when it represents 4–5% of the average values against 2% for CT.

Long-term energy and water balances

Figure 3 presents the average pixel values and standard deviations (SD) for net radiation – R_n (Fig. 3a) and its partition into latent – λE (Fig. 3b), sensible – H (Fig. 3c), and ground – G (Fig. 3d) heat fluxes, at the MOD13Q1 16-day timescale, for the long-term period from 2007 to 2021, in terms of Day of the Year (DOY). Data are classified for the Atlantic Forest (AF) and Caatinga (CT) biomes, within the SEALBA agricultural growing region.

The long-term R_n values (Fig. 3a) range from 6.50 to 11.50 MJ m^{-2} d^{-1}, with the highest averages at the start and at the end of the year, while the lowest ones are at the middle of the year, for both AF and CT, however slightly higher for CT. At the annual scale, the R_n rates in AF were 99% of those for CT, with the largest spatial variations for AF at the start of the year, according to the SD values. Crossing Figs. 2b and 3a, the ratio R_n/R_G ranges from 0.44 from May to June (DOY 145–160) to 0.52 from August to September (DOY 241–256). During this last period occur conditions

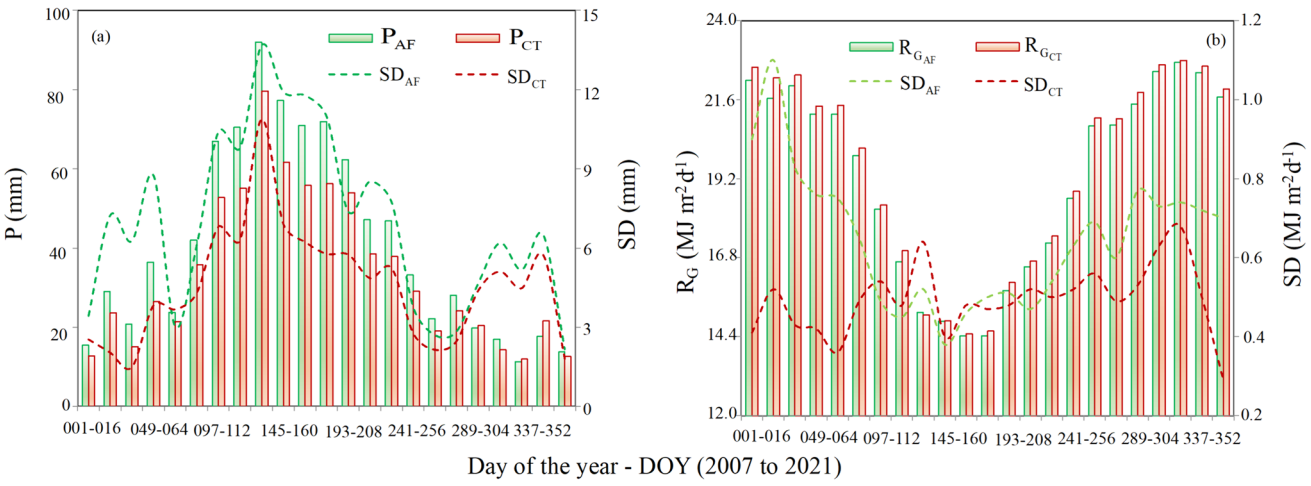

Fig. 2 Average pixel values and standard deviations (SD) for precipitation – P (**a**) and global solar radiation—R_G (**b**), at the MOD13Q1 reflectance 16-day timescale, for the Atlantic Forest (AF) and Caatinga (CT) biomes, within the SEALBA agricultural growing region, for the long-term period from 2007 to 2021, in terms of Day of the Year (DOY)

of higher available energy, at the end of the rainy season, when the root-zones are still under good moisture conditions, favorable for λE.

Regarding the R_n partition into λE, stronger differences between the AF and CT biomes arise (Fig. 3b). The largest λE rates are for AF at the start and at the end of the year, just after the rainy periods (see also Fig. 2a). The average λE is between 3.80 and 6.80 MJ m^{-2} d^{-1} for AF and from 2.20 to 7.20 MJ m^{-2} d^{-1} for CT, with average annual values of 5.10 MJ m^{-2} d^{-1} and 4.00 MJ m^{-2} d^{-1}, respectively, being the rates for AF 26% higher than those for CT. However, from June (DOY 177) to August (DOY 224), the end the rainy season, the CT species present λE rates larger than those for AF, period when the root-zone moisture is not limited for both biomes. The highest λE spatial variations happen from January to March (DOY 001–064) and from November to December (DOY 305–352), in both biomes, when the SD values surpass 50% of the average pixel values. At the annual scale SD represents 33% of the average λE for CT, while this percentage is 28% for AF. The annual λE/R_n values were 0.54 and 0.43 for AF ad CT, respectively, however, inside the rainy period this ratio is higher than 0.80 for both biomes, indicating the best root-zone moisture conditions for rainfed agriculture, while outside this period this ratio falls to 0.34 and 0.20 for AF and CT, respectively, meaning higher water stress conditions for CT and irrigation needs for crops.

The highest H values are at the start and at the end of the year (Fig. 3c), with averages above 6.00 MJ m^{-2} d^{-1} in AF and higher than 8.00 MJ m^{-2} d^{-1} in CT, from January to February (DOY 001–048). The lowest H rates, with average below 1.00 MJ m^{-2} d^{-1} occur from June to July (DOY 161–208). Although in general CT presents larger H values than those for AF, there is a short period when they are

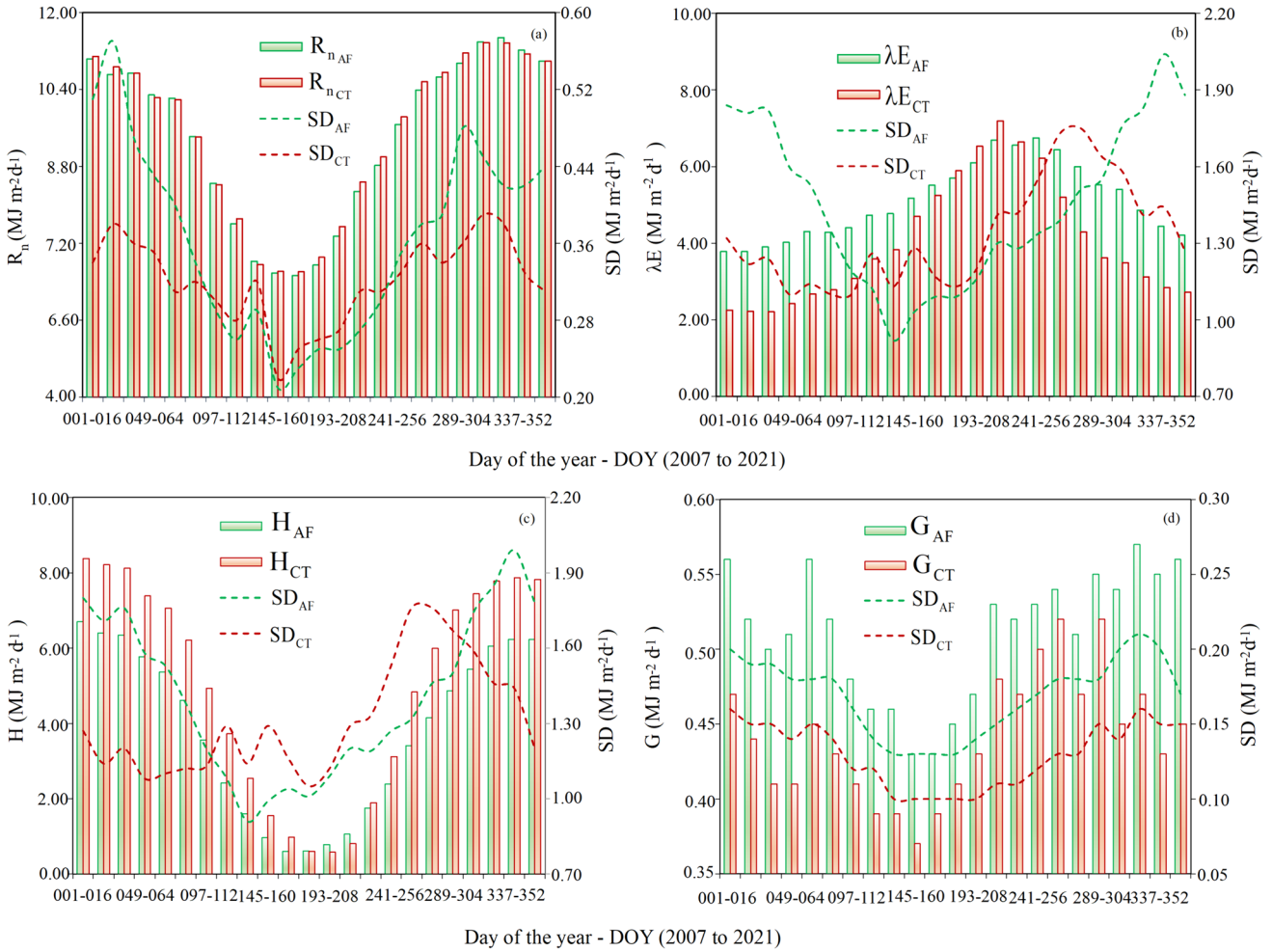

Fig. 3 Average values and standard deviations (SD), of the energy balance components at the 16-day MODIS timescale in terms of Day of the Year (DOY), for the long-term period from 2007 to 2021. Data are classified for the Atlantic Forest (AF) and Caatinga (CT) biomes, within the SEALBA agricultural growing region. **a** net radiation – R_n; **b** latent heat flux – λE; **c** sensible heat flux – H; **d** ground heat flux – G

slightly lower, from June to August (DOY 177–224). At the annual scale CT presents a daily average H of 5.00 MJ m^{-2} d^{-1}, 32% higher than that for AF (3.80 MJ m^{-2} d^{-1}). More H spatial variations happen in AF than in CT, with SD representing 37 and 26% of the average values, respectively, at the annual scale. Inside the rainy period the H/R_n ratio drops to below 0.20 in both biomes, indicated good conditions for rainfed agriculture, while outside this period, at the start and at the end of the year, this ratio is above 0.55 and 0.75 for AF and CT, respectively, meaning higher warming and water stress conditions for CT.

Among the energy balance components in SEALBA, G is the lowest one (Fig. 3d). Although its amplitude along the year is not large, there are some differences between the biomes, being the minimum average values 0.43 and 0.37 MJ m^{-2} d^{-1} for AF and CT, respectively, from May to June (DOY 145–160), while the corresponding maximums are 0.57 MJ m^{-2} d^{-1} in AF, from November to December (DOY 321–336) and 0.52 MJ m^{-2} d^{-1} in CT, from October to November (DOY 289–304). At the annual scale, the daily average G in AF is 16% higher than that for CT and the SD values for AF represent 33% of the mean pixel value, while for CT this percentage is 29%. Regarding the G/R_n ratio, it was very small for both biomes, ranging from 0.04 to 0.07, with this high end being for AF.

Having the pixel values for λE and the available energy (R_n – G), Ef was calculated classifying the biomes AF and CT (Eq. 13) and considered representative of the root-zone moisture conditions. The long-term annual Ef values (2007–2021) were 0.60 for AF and 0.48 for CT, being the highest values in 2020, when the average for the SEALBA agricultural growing region was 0.62, while the lowest ones happened in driest year 2018, when it was 0.48.

Standardized index for the energy balance components

To test the monitoring of anomalies on the energy and water balance conditions along the years, we used the standardized index (STD) for latent heat fluxes (λE_{STD}), sensible heat fluxes (H_{STD}), and evaporative fraction (Ef_{STD}), at the 16-day MODIS timescale, considering the average pixel values of these STDs from 2018 to 2021 in terms of Day of the Year (DOY), classifying the AF and CT biomes within SEALBA, for the respective long-term periods of 2007–2018, 2007–2019, 2007–2020, and 2007–2021.

Standardized index for latent heat flux

Figure 4 shows the λE_{STD} values during 2018 (Fig. 4a), 2019 (Fig. 4b), 2020 (Fig. 4c), and 2021 (Fig. 4d), at the MODIS 16-day timescale in terms of Day of the Year (DOY), classifying the Atlantic Forest (AF) and Caatinga (CT) biomes within SEALBA, regarding the respective long-term periods 2007–2018, 2007–2019, 2007–2020, and 2007–2021.

The positive λE_{STD} average values for 2018 (Fig. 4a) were concentrated from January to July (DOY 001–208) for both AF and CT, meaning water fluxes higher than those for the long-term conditions 2007–2018, with the peaks of 0.77 happening in March (DOY 065–080) for AF and 0.45 in January (DOY 001–016) for CT. Regarding the negative λE_{STD} values, translating lower water fluxes than those for the long-term periods, their concentrations were from August to December (DOY 225–352), with the lowest ones of -0.69 for AF from November to December (DOY 321–336) and -1.04 for CT in September (DOY 257–272).

Considering 2019 and the long-term period 2007–2019 (Fig. 4b), the highest positive average λE_{STD} for AF of 0.56 was from April to May (DOY 113–128), while for CT of 0.92 it happened in August (DOY 225–240), periods under the highest water fluxes compared to the long-term periods. The most negative λE_{STD} values for both biomes occurred from February to March (DOY 049–064), averages of -0.30 and -0.67 for AF and CT, respectively, the lowest water fluxes compared to the long-term periods.

Analyzing λE_{STD} for 2020, regarding the long-term period 2007–2020 (Fig. 4c), it was detected fewer negative average values, when comparing with the previous analyzed years, for both, AF and CT, occurring only from January to March (DOY 001–080) and from October to November (DOY 289–320). Thus, during this year, water fluxes were, in general, higher than those for the long-term period in the whole SEALBA. The highest positive λE_{STD} values for both biomes were in April (DOY 097–112), averaging 0.49 and 0.85 for AF and CT, respectively. The most negative ones, averaging -0,43, happened in October for AF (DOY 289–304) and of -0.27 in January for CT (DOY 001–016), short periods with lower water fluxes comparing with the long-term conditions.

For the year 2021 (Fig. 4d), half of the λE_{STD} values for AF (52%) and the majority for CT (61%) were negative, evidencing several lower water fluxes periods from vegetation along the year when comparing with the long-term periods from 2007 to 2021. However, positive values happened at the end of the year, with the highest averages of 0.42 and 0.41 for AF and CT, respectively, in December (DOY 337–365), with water fluxes above than those for the long-term periods. The lowest mean λE_{STD} pixel values for both biomes were in March (DOY 065–080), -0.28 and -0.50 for AF and CT, respectively, indicating lower water fluxes around this month, when comparing with the long-term periods.

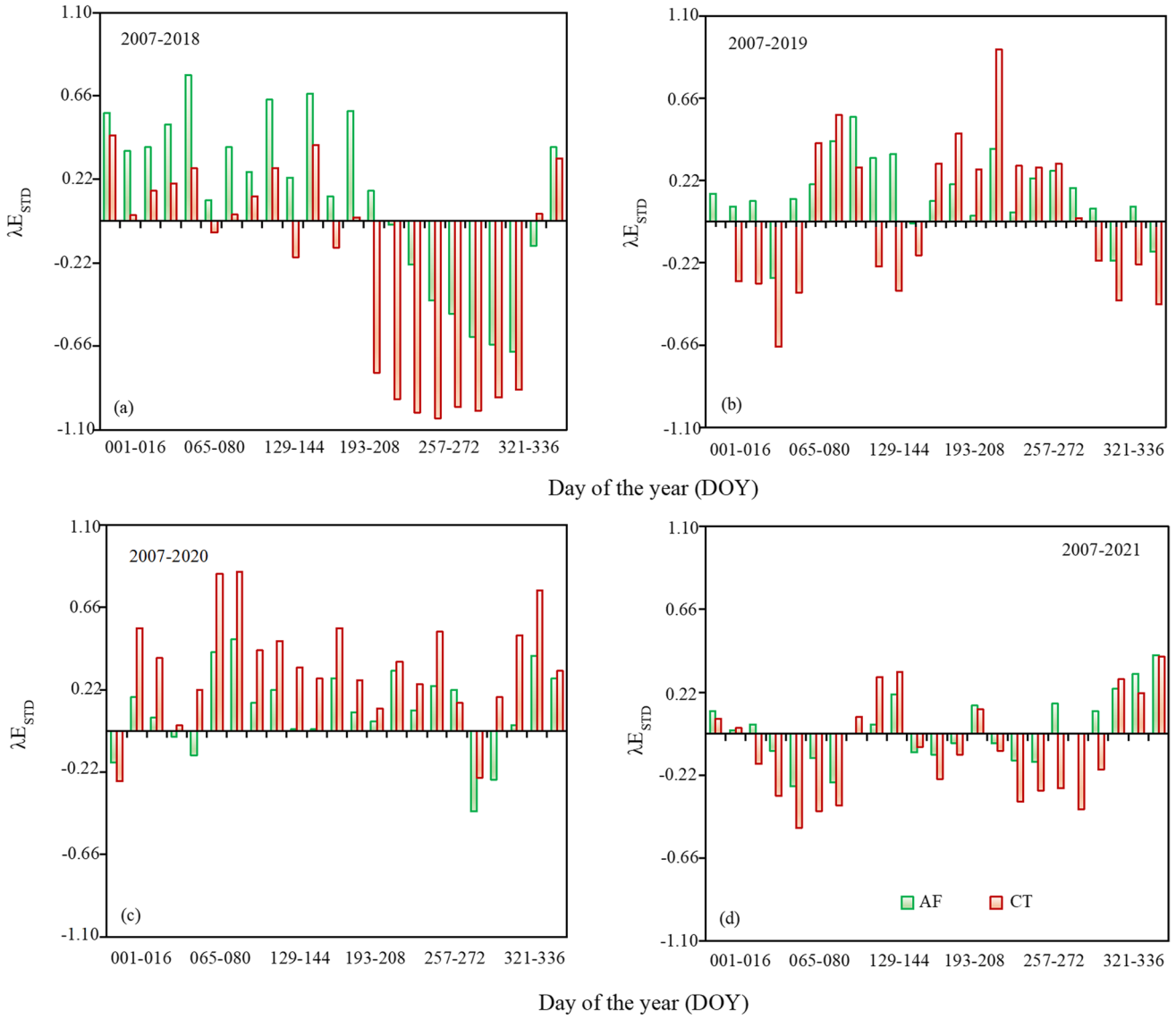

Fig. 4 Average values of the standardized index for latent heat fluxes (λE_{STD}) during 2018 (**a**), 2019 (**b**), 2020 (**c**), and 2021 (**d**), at the MODIS 16-day timescale in terms of Day of the Year (DOY), classifying the Atlantic Forest (AF) and Caatinga (CT) biomes within the SEALBA agricultural growing region, regarding the respective long-term periods 2007–2018, 2007–2019, 2007–2020, and 2007–2021

Standardized index for sensible heat flux

Figure 5 shows the H_{STD} values during 2018 (Fig. 5a), 2019 (Fig. 5b), 2020 (Fig. 5c), and 2021 (Fig. 5d), at the MODIS 16-day timescale in terms of Day of the Year (DOY), classifying the Atlantic Forest (AF) and Caatinga (CT) biomes within SEALBA, regarding the respective long-term periods 2007–2018, 2007–2019, 2007–2020, and 2007–2021.

Considering the year 2018 (Fig. 5a), the positive H_{STD} values for both AF and CT, were concentrated during the second half of the year (DOY 209–365). The highest averages of 0.80 and 1.23 for AF and CT, respectively, occurred from September to October (DOY 273–304), period of the warmest conditions, when compared to the long-term conditions from 2007 to 2018. The most negative mean pixel values were from February to March, reaching to -0.51 and -0.26 in AF and CT, respectively, indicating cooling situations, when the H fluxes were lower than the long-term values, mainly in AF.

Regarding 2019 (Fig. 5b), the positive H_{STD} values occurred in two periods of the year for both biomes, from January to March (DOY 017–080) and from October to December (DOY 289–365), while the most negative ones were from March to October (DOY 081–288), with the lowest averages for CT. The positive peaks were between January and February (DOY 017–032), outside the rainy season, around 0.79

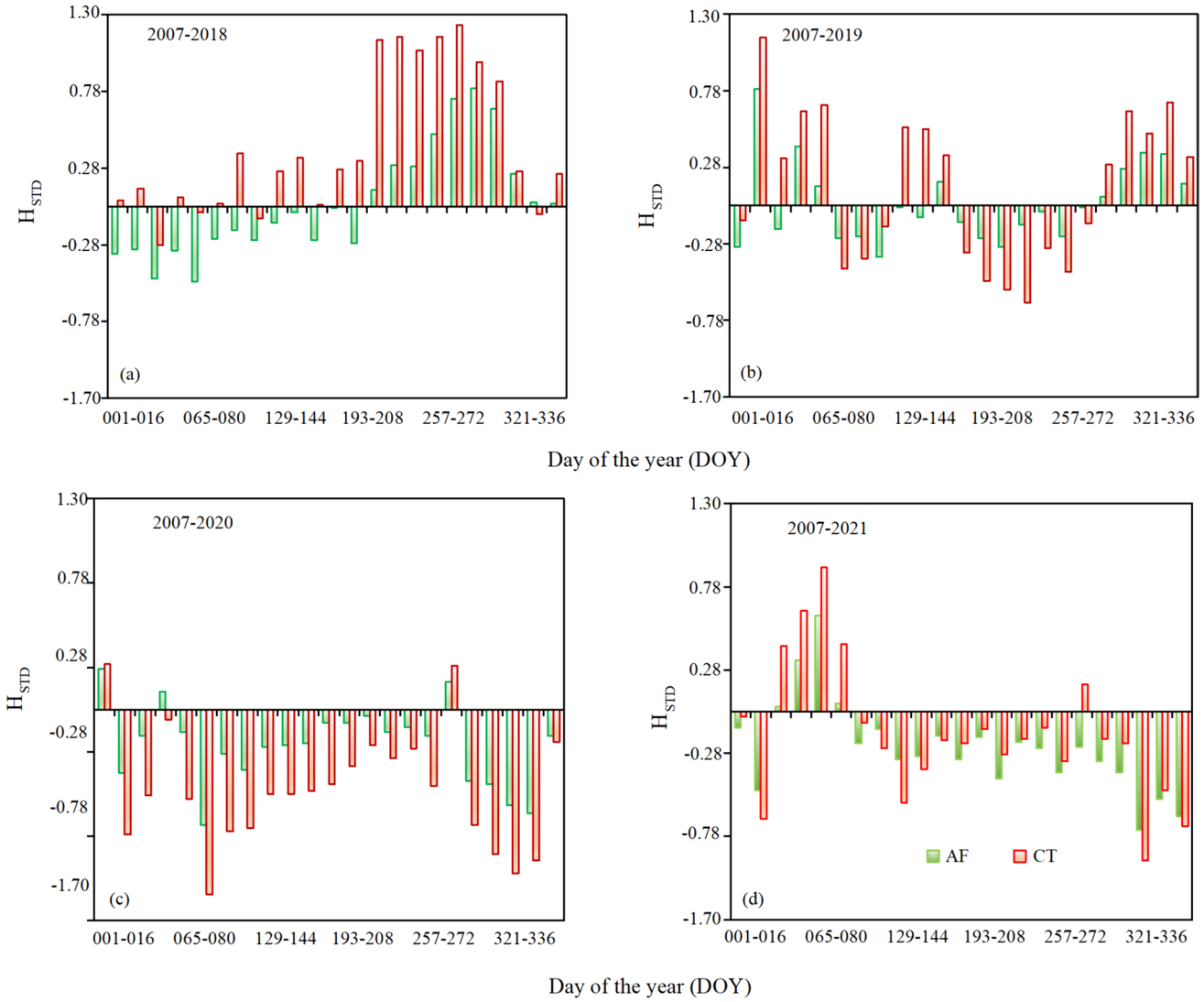

Fig. 5 Average values of the standardized index for sensible heat fluxes (H_{STD}) during 2018 (**a**), 2019 (**b**), 2020 (**c**), and 2021 (**d**), at the MODIS 16-day timescale in terms of Day of the Year (DOY), classifying the Atlantic Forest (AF) and Caatinga (CT) biomes within the SEALBA agricultural growing region, regarding the respective long-term periods 2007–2018, 2007–2019, 2007–2020, and 2007–2021

and 1.14 for AF and CT, respectively, when occurred H fluxes above the long-term rates, indicating the warmest conditions. The most negative average values were -0.35 for AF from April to May (DOY 113–128) and -0.66 for CT in August (DOY 225–240), when the fluxes were lower than the long-term values, evidencing the coolest situations, mainly for CT, after the rainy season (see also Fig. 2a).

Analyzing the H_{STD} values for 2020 (Fig. 5c), there were very fewer positive average values for both AF and CT, comparing with the previous analyzed years, happening only at the start of January (DOY 001–016) and from September to October (DOY 273–288). This means that most of the H rates were lower than those for the long-term conditions, meaning cooling conditions during this year. The lowest average H_{STD} values for both biomes of -0.71 and -1.14, for AF and CT, respectively, were from March to April (DOY 081–096), period with H fluxes much below the long-term values from 2007 to 2020.

For the year 2021 (Fig. 5d), only from February to April (DOY 033–096) occurred positive H_{STD} values for both AF and CT, reaching to respective averages of 0.60 and 0.90, what means that for this year, most of the H fluxes were also below of those for the long-term conditions 2007–2021, indicating general cooling situations, with the lowest averages of -0.74 and -0.93, respectively for AF and CT, from November to December (DOY 321–336).

Standardized index for evaporative fraction

Figure 6 shows the Ef_{STD} values during 2018 (Fig. 6a), 2019 (Fig. 6b), 2020 (Fig. 6c), and 2021 (Fig. 6d), at the MODIS 16-day timescale in terms of Day of the Year (DOY), classifying the Atlantic Forest (AF) and Caatinga (CT) biomes within SEALBA, regarding the respective long-term periods 2007–2018, 2007–2019, 2007–2020, and 2007–2021.

In 2018 (Fig. 6a), the Ef_{STD} positive values for both biomes were concentrated from January to the end of July (DOY 001–208), reaching to peaks of 0.64 and 0.38, for AF and CT, respectively, meaning higher root-zone moisture conditions than those for the long-term values of 2007–2018, favorable for rainfed agriculture. The most negative of -0.66 for AF and -1.07 for CT, happened from September to October (DOY 257–304), when the root-zone moisture levels were much lower than the long-term ones, translated into much supplementary irrigation water needs for crops.

Considering the year 2019 (Fig. 6b), the positive Ef_{STD} values were concentrated from March to May (DOY 081–128), when in AF the average reached to 0.40, and from June to September (DOY 177–256), when occurred the peak of 0.57 in CT, indicating better root-zone moisture conditions for crops than those for the long-term periods (2007–2019). The lowest Ef_{STD} values occurred from February to March (DOY 049–064), with the averages dropping to -0.37 and—0.69 in AF and CT, respectively, when the root-zone moisture levels were much below than those for long-term periods, evidencing more irrigation water requirements for agriculture.

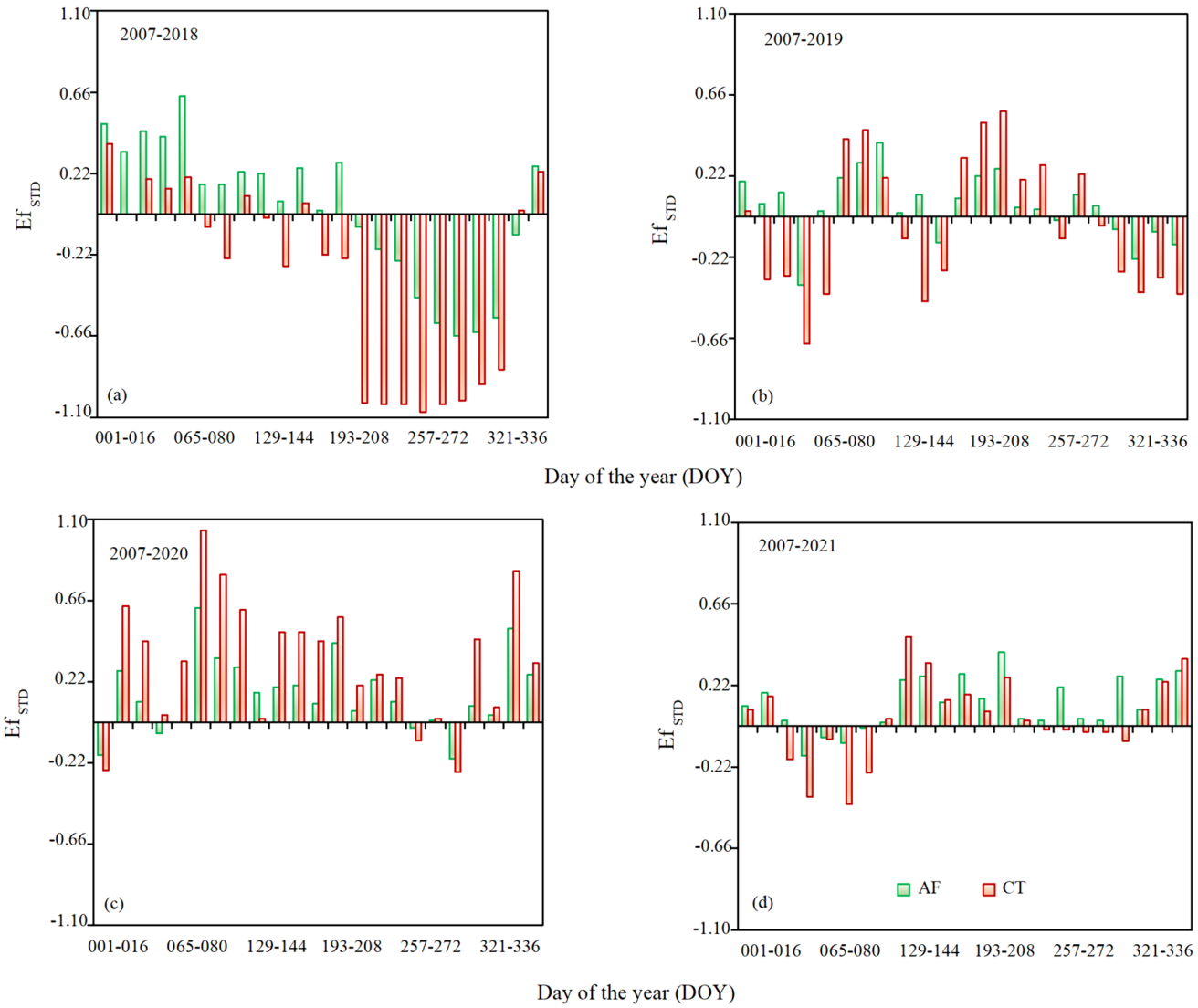

Fig. 6 Average values of the standardized index for evaporative fraction (Ef_{STD}) during 2018 (**a**), 2019 (**b**), 2020 (**c**), and 2021 (**d**), at the MODIS 16-day timescale in terms of Day of the Year (DOY), classifying the Atlantic Forest (AF) and Caatinga (CT) biomes within the SEALBA agricultural growing region, regarding the respective long-term periods 2007–2018, 2007–2019, 2007–2020, and 2007–2021

Analyzing the Ef_{STD} average values for 2020, regarding the long-term period from 2007 to 2020 (Fig. 6c), it was detected fewer negative ones for both AF and CT, meaning good root-zone conditions during this year. The highest average Ef_{STD} values of 0.62 and 1.04, for AF and CT, respectively, were from March to May (DOY 081–096), periods with the best root-zone moisture levels comparing with the long-term conditions, meaning no irrigation needs for crops. Regarding the lowest averages, respectively -0.20 and -0.27 for AF and CT, they were in October (DOY 289–304), picturing slightly lower root-zone moisture levels comparing with the long-term conditions.

For the year 2021 (Fig. 6d), the majority of the average Ef_{STD} values for both AF and CT were positive or close to zero, but with few occasions in the first half of the year when they were negative, mainly for CT, picturing slightly water deficits for crops. The highest averages of 0.40 and 0.48 for AF and CT, respectively, occurred from May to August (DOY 129–224), during the rainy season, indicated very good root-zone moisture for rainfed agriculture and no need of irrigation. The lowest Ef_{STD} values, for both biomes, were February to April (DOY 049–096), before the rainy period, when there were some degrees of water scarcity.

Discussion

Effects of the energy and water balances on vegetation conditions

Drops on precipitation values together with increasing solar radiation levels at the start and at the end of the year reduces the partition of R_n into λE, increasing H, promoting declines on vegetation activity (Sun et al. 2015). The R_n values in SEALBA follow those for R_G, independently of the rainfall amounts (see Figs. 2 and 3a), with the highest values at the start and at the end of the year ($R_n/R_G = 0.52$) and the lowest ones in the middle of the year ($R_n/R_G = 0.44$), for both the Atlantic Forest (AF) and Caatinga (CT) biomes**.** By field energy balance experiments from 2011 to 2012 in AF, within the Brazilian Southeast region, Funari and Filho (2014) found R_n/R_G values from 0.40 to 0.68. Through Landsat measurements in CT within Northeast Brazil, Teixeira et al. (2017a) reported R_n/R_G ratio ranging from 0.41 to 0.47. These previous values are inside of our results.

The largest λE rates for both AF and CT, are just after the rainy seasons, when $\lambda E/R_n$ is above 0.80, while the respective lowest ratios of 0.34 and 0.20 occur during the driest conditions, independently of the solar radiation rates (Figs. 2b and 3b). From micrometeorological measurements in AF, Guauque-Melado et al. (2022) reported higher $\lambda E/R_n$ values from 0.86 to 0.88, but these authors neglected the fraction of R_n partitioned into G, while Funari and Filho (2014), also with micrometeorological measurements in this biome, found daily $\lambda E/R_n$ values between 0.47 to 0.65, inside our annual value ($\lambda E/R_n = 0.54$). From energy balance techniques in CT, da Silva et al. (2017) reported average $\lambda E/R_n$ ranging from 0.23 to 0.41 for the dry and rainy periods, respectively. With also energy balance methods in CT, Campos et al. (2019) found an annual $\lambda E/R_n$ value of 0.20, like our one during the driest conditions.

The highest H values are at the start and at the end of the year at low rainfall amounts, when H/R_n is above 0.55 and 0.75 for AF and CT, respectively, while the lowest ones occur during the rainy season, in the middle of the year, when this ratio is below 0.20 for both biomes (Fig. 3c). Thus, these warmer conditions outside the rainy seasons lead to a reduction of available water resources from November to February (Huang et al. 2017; Vicente-Serrano et al. 2018; Yang et al. 2016). From field energy balance measurements in AF, inside the Brazilian Southeast region, Guauque-Melado et al. (2022) reported H/R_n ranging from 0.12 to 0.14, much lower than our ratios in Northeast Brazil. However, also from micrometeorological measurements in AF, Funari and Filho (2014) found H/R_n values from 0.25 to 0.42, inside our ranges. The H/R_n values for CT in the current study are much larger than those reported by Teixeira et al. (2021a) from Landsat measurements in irrigated lemon crop inside this biome, who found annual averages of 0.30, 0.16, and 0.01 under drip, micro sprinkler, and pivot irrigation systems, respectively. These last lower values can be explained by the frequent occurrence of heat advection from the hotter areas at the vicinities of irrigated plots, increasing λE while reducing H in irrigated plots (Consoli and Papa 2013). However, Campos et al. (2019), also from energy balance measurements in CT, reported H/R_n annual values of 0.50, like our average value of 0.53 for this biome.

Even the amplitude in G values not being large and without strong differences between the biomes, the minimum values, for both, are at the middle of the year, while the maximums are at the end of the year, yielding small annual G/R_n values of 0.04 to 0.07, for CT and AF, respectively (Fig. 3d). From energy balance measurements in AF within the Brazilian Southeast region, Funari and Filho (2014) found G/R_n values from 0.03 to 0.24. The high end of this range is much larger than our ones for AF, but their rates involved urban areas of the big São Paulo city. However, da Silva et al. (2017) reported a low average G/R_n value of 0.03. Under dry and wet conditions in CT, Campos et al. (2019) found G/R_n values between -0.04 to 0.04. The negative values, at shorter timescales, mean heat advection from the warmer vicinities to the wetter measured area (Teixeira et al. 2021a).

After accounting the energy balance components, the root zone moisture was evaluated through the evaporative fraction (Ef), using Eq. 13. Larger Ef values for AF than for CT, indicates better moisture conditions for rainfed agriculture and

less irrigation needs in the first biome, but with magnitudes varying along the seasons and years. These long-term assessments are important for environmental policies because they picture the patterns of the energy and mass fluxes between vegetation and the lower atmosphere. However, it is also important to analyse how a specific period along the year is being altered regarding the long-term conditions. This was done by testing the standardized index for these energy balance components from 2018 to 2021 (Eq. 14).

Applicability of energy and water balance standardized indices for vegetation and agricultural monitoring

The energy fluxes used for evapotranspiration can be strongly variable along the years, for both, AF and CT biomes, alternating positive and negative λE_{STD} values, without specific trends. Reductions on λE (negative λE_{STD}), impact rainfed agriculture while increasing λE (positive λE_{STD}), although being favorable for biomass production, may means less water availability for other water users (Teixeira et al. 2013). Among the analyzed years, the most negative λE_{STD} values were for CT in 2018 (Fig. 4a), indicating several periods of lower water fluxes, regarding the long-term conditions (2007–2018), while the most positive λE_{STD} values were detected for AF in 2019 (Fig. 4b), evidencing higher water fluxes, considering the long-term period 2007–2019. The λE_{STD} values around zero during 2021 indicated that λE rates in this year was more like those for the long-term conditions from 2007 to 2021 (Fig. 4d). According to Guauque-Melado et al. (2022), distinct biomes respond differently to water availability, depending on the weather conditions, as the case of CT, where the species develop physiological adaptations to overcome water scarcity (Marques et al. 2020). Detection of λE anomalies is appropriate for sustainable environmental ecosystem monitoring because they represent the alterations on the real water consumptions from vegetated surfaces (Huang et al. 2016; Teixeira et al. 2021b; Xu et al. 2013; Yang et al. 2018; Zhang et al. 2019; Zhang et al. 2021).

Regarding the sensible heat fluxes (H), it is detected the strong warming and cooling variations among surfaces and the lower atmosphere for both biomes, AF and CT. The most negative average H_{STD} was for CT in 2020 (Fig. 5c), indicating several situations below the long-term from 2007 to 2020, while the most positive one was also for CT in 2018 (Fig. 5a), translated more warm conditions above those for 2007–2018. The H_{STD} values for the years 2019 and 2021 around zero (Fig. 5b and d, respectively) indicated similarity with the long-term heating/cooling situations (2007–2019 and 2007–2021). According to Teixeira et al. 2017a, 2021a), increasing positive H means warmer conditions, while lower H, including the negative values, mean more cooling situations. These H_{STD} values allow to analyze how much, during the years 2018, 2019, 2020, and 2021, the air heating/cooling conditions differed from those for the long-term period (2007–2018, 2007–2019, 2007–2020, and 2007–2021), as in case of other environmental parameters (Teixeira et al. 2021b; Zhang et al. 2019, 2021). These effects on vegetation growth are variable according to seasons (Wolf et al. 2016), with the contribution of H increasing when the system changes from energy to water limited along and inside the years (Marques et al. 2020).

The dynamics of the Ef_{STD} values allow to analyze how much, during the analyzed years, the root-zone moisture conditions differed from those for the long-term periods (Teixeira et al. 2021b; Zhang et al. 2019, 2021). Increasing Ef means higher root-zone moisture levels for vegetation (Teixeira et al. 2021a), while lower Ef values identify water stress (Lu et al. 2011). The most negative Ef_{STD} was for CT in 2018 (Fig. 6a), with an average value of -0.94, indicating several water scarcity situations, but the highest positive one was also for CT in 2020 (Fig. 6c), with a mean STD of 1.08, translating better root-zone moisture levels. In general, higher Ef_{STD} values were observed for AF than for CT, with exception for the year 2020. According to Zhou and Zhou (2009), air humidity and the available energy, were the most important variables for the root-zone moisture variations in a reed marsh in Northeast China. However, Ef_{STD} values in plants under non-optimum moisture levels, are also influenced by the stomatal regulation (Mata-González et al. 2005; Mateos et al. 2013), mechanism much noticed for the CT species. Therefore, Ef_{STD} is an important water parameter for vegetation activity, as root-zone moisture influences crop growth and agricultural production (Seddon et al. 2016; Zhang et al. 2021).

Based on the long-term energy balance assessments (2007–2021), as well as on their anomalies through the standardized indices, from 2018 to 2021, it is concluded that latent and sensible fluxes, and then the root-zone moisture conditions, may strongly vary among years and seasons, being noticed a memory effects (De Keersmaecker et al. 2015) for both Brazilian biomes inside the SEALBA agricultural growing region. However, water availability to the root zones, represented by Ef, is higher for AF than that for CT, as changes in vegetation canopies vary between their species, according to environmental conditions (Zhang et al. 2016), and canopy changes are higher in CT than in AF during water stress events (Aires et al. 2008).

Overall, the energy balance modelling with the MOD13Q1 reflectance product, can be used to investigate the anomalies on water availability conditions along the years in distinct biomes. These assessments are important for rational agricultural management as they may show suitable periods and places for rainfed crops as well as the irrigation needs for irrigated agriculture along specific seasons of a year, while helping to minimize competitions among other water users. As future research directions it is recommended

to test the SAFER's equations with simultaneous MODIS and micrometeorological measurements in other environmental conditions to check the need of calibrations for its modelling equations.

Conclusions

Net radiation (R_n) values follow the solar radiation levels in the SEALBA region, however slightly higher for the Caatinga (CT) than for the Atlantic (AF) biome. Significant differences are detected on R_n partitions into latent (λE), sensible (H), and ground (G) fluxes between AF and CT, promoting distinct root-zone moisture conditions, represented by the evaporative fraction (Ef). The largest λE and lowest H values are for AF at the start and at the end of the year, outside the rainy seasons.

On one hand, among the analyzed years, the most negative standardized index (STD) values for λE and Ef and positive for H, were in CT during the second half of 2018, when occurred several periods of lower water fluxes and water availability for vegetation together with higher warming conditions, unfavorable for rainfed agriculture and requiring more irrigation water for irrigated agriculture. On the other hand, the most positive STD values for λE and Ef and negative for H, were detected also for CT in 2020, occurring higher water fluxes and water availability for vegetation, together with more cooling situations, favorable for rainfed agriculture and requiring less irrigation water for irrigated agriculture.

These long-term energy and water balance assessments being carried out year after year, have potential to support environmental management as they picture suitable periods and places for rainfed agriculture as well as the irrigation needs for crops, allowing rational agricultural water management while minimizing environmental impacts and water competitions among other water users under climate and land-use changes conditions. To use this monitoring system in other environmental conditions, it is recommended to test the SAFER's equations with simultaneous MODIS and micrometeorological measurements to check the need of calibrations of the modelling equations.

References

Aires LMI, Pio CA, Pereira JS (2008) Carbon dioxide exchange above a Mediterranean C3/C4 grassland during two climatologically contrasting years. Glob Chang Biol 14:539–555. https://doi.org/10.1111/j.1365-2486.2007.01507.x

Allen RG, Tasumi M, Morse A, Trezza R, Wright JL, Bastiaanssen WGM, Kramber W, Lorite I, Robison CW (2007) Satellite-based energy balance for mapping evapotranspiration with internalized calibration (METRIC) - applications. J Irrig Drain Eng 133:395–406. https://doi.org/10.1061/(ASCE)0733-9437(2007)133:4(380)

Allen RG, Pereira LS, Raes D, Smith M (1998) Crop evapotranspiration, guidelines for computing crop water requirements, FAO irrigation and drainage paper 56. FAO, Rome

Almeida SL de, Souza JB, Pilon C, de Castro Teixeira AH, dos Santos AF, Sysskind MN, Vellidis G, da Silva RP (2023) Performance of the SAFER model in estimating peanut maturation. Eur J Agron 147:126844. https://doi.org/10.1016/j.eja.2023.126844

Araujo LM, de Castro Teixeira AH, Bassoi LH (2019) Evapotranspiration and biomass modelling in the Pontal Sul irrigation scheme. Int J Remote Sens. https://doi.org/10.1080/01431161.2019.1688416

Bastiaansssen WGM, Menenti M, Feddes RA, Roerink GJ, Holtslag AAM (1998) A remote sensing surface energy balance algorithm for land (SEBAL) 1. Formulation. J Hydrol 212–213:198–212. https://doi.org/10.1016/S0022-1694(98)00253-4

Beguería S, Vicente-Serrano SM, Reig F, Latorre B (2014) Standardized precipitation evapotranspiration index (SPEI) revisited: parameter fitting, evapotranspiration models, tools, datasets and drought monitoring. Int J Climatol 34:3001–3023. https://doi.org/10.1002/joc.3887

Bento VA, Gouveia CM, Dacamara CC, Trigo IF (2018) A climatological assessment of drought impact on vegetation health index. Agric For Meteorol 259:286–295. https://doi.org/10.1016/j.agrformet.2018.05.014

Bhattarai N, Wagle P, Gowda PH, Kakani VG (2017) Utility of remote sensing-based surface energy balance models to track water stress in rain-fed switchgrass under dry and wet conditions. ISPRS J Photogramm Remote Sens 113:128–141. https://doi.org/10.1016/j.isprsjprs.2017.10.010

Brouwers NC, van Dongen R, Matusick G, Coops NC, Strelein G, Hardy G (2015) Inferring drought and heat sensitivity across a Mediterranean forest region in southwest Western Australia: a comparison of approaches. Forestry 88:454–464. https://doi.org/10.1093/forestry/cpv014

Campos S, Mendes KR, da Silva LL, Mutti PR, Medeiros SS, Amorim LB, dos Santos CAC, Perez-Marin AM, Ramos TM, Marques TV, Lucio PS, Costa GB, Santos e Silva CM, Bezerra BG (2019) Closure and partitioning of the energy balance in a preserved area of a Brazilian seasonally dry tropical forest. Agric For Meteorol 271:398–412. https://doi.org/10.1016/j.agrformet.2019.03.018

Cleugh HA, Leuning R, Mu Q, Running SW (2007) Regional evaporation estimates from flux tower and MODIS satellite data. Remote Sens Environ 106:285–304. https://doi.org/10.1016/j.rse.2006.07.007

Consoli S, Papa R (2013) Corrected surface energy balance to measure and model the evapotranspiration of irrigated orange orchards in semi-arid Mediterranean conditions. Irrig Sci 31:1159–1171. https://doi.org/10.1007/s00271-012-0395-4

Consoli S, Vanella D (2014) Comparisons of satellite-based models for estimating evapotranspiration fluxes. J Hydrol 513:475–489. https://doi.org/10.1016/j.jhydrol.2014.03.071

Consoli S, Licciardello F, Vanella D, Pasotti L, Villani G, Tomei F (2016) Testing the water balance model CRITERIA using TDR measurements, micrometeorological data, and satellite-based information. Agric Water Manag 170:68–80. https://doi.org/10.1016/j.agwat.2015.11.003

da Silva PF, de Sousa Lima JR, Antonino ACD, Souza R, de Souza ES, Silva JRI, Alves EM (2017) Seasonal patterns of carbon dioxide, water, and energy fluxes over the Caatinga and grassland in the semi-arid region of Brazil. J Arid Environ 147:71–82. https://doi.org/10.1016/j.jaridenv.2017.09.003

De Keersmaecker W, Lhermitte S, Tits L, Honnay O, Somers B, Coppin P (2015) A model quantifying global vegetation resistance and resilience to short-term climate anomalies and their relationship with vegetation cover. Glob Ecol Biogeogr 24:539–548. https://doi.org/10.1111/geb.12279

Ford TW, Labosier CF (2017) Meteorological conditions associated with the onset of flash drought in the Eastern United States. Agric

For Meteorol 247:414–423. https://doi.org/10.1016/j.agrformet.2017.08.031
Funari FL, Filho AJP (2014) Energy balance in a patch of the Atlantic Forest in São Paulo City. Brazil J Water Res Prot 6:805–812. https://doi.org/10.4236/jwarp.2014.69076
Gouveia C, Trigo RM, Beguería S, Vicente-Serrano SM (2017) Drought impacts on vegetation activity in the Mediterranean region: an assessment using remote sensing data and multi-scale drought indicators. Glob Planet Change 151:15–27. https://doi.org/10.1016/j.gloplacha.2016.06.011
Guauque-Melado D, Rodrigues A, Terra M, Yanagi S, Diotto A, de Mello C (2022) Evapotranspiration under drought conditions: the case study of a seasonally dry Atlantic Forest. Atmosphere 13:871. https://doi.org/10.3390/atmos13060871
Hao Z, AghaKouchak A (2013) Multivariate Standardized Drought Index: a parametric multi-index model. Adv Water Resour 57:12–18. https://doi.org/10.1016/j.advwatres.2013.03.009
Huang J, Yu H, Guan X, Wang G, Guo R (2016) Accelerated dryland expansion under climate change. Nat Clim Chang 6:166. https://doi.org/10.1038/nclimate2837
Huang S, Li P, Huang Q, Leng G, Hou B, Ma L (2017) The propagation from meteorological to hydrological drought and its potential influence factors. J Hydrol 547:184–195. https://doi.org/10.1016/j.jhydrol.2017.01.041
Jardim AMRF, Júnior GNA, da Silva MV, dos Santos A, da Silva JLB, Pandorfi H, de Oliveira-Júnior JF, de Castro Teixeira AH, Teodoro PE, de Lima JLPM, Junior CAS, Souza LSB, Silva EA, Silva TGFS (2022) Using remote sensing to quantify the joint effects of climate and land use/land cover changes on the Caatinga biome of Northeast Brazilian. Remote Sens 14:1911. https://doi.org/10.3390/rs14081911
Kim D, Rhee J (2016) A drought index based on actual evapotranspiration from the Bouchet hypothesis. Geophys Res Lett 43:10277–10285. https://doi.org/10.1002/2016GL070302
Lewinsohn TM, Prado PI (2005) How many species are there in Brazil? Conserv Biol 19:619–624. https://doi.org/10.1111/j.1523-1739.2005.00680.x
Lu N, Chen S, Wilske B, Sun G, Chen J (2011) Evapotranspiration and soil water relationships in a range of disturbed and undisturbed ecosystems in the semi-arid Inner Mongolia, China. J Plant Ecol 4:49–60. https://doi.org/10.1093/jpe/rtq035
Mariano DA, dos Santos CAC, Wardlowa BD, Anderson MC, Schiltmeyera AV, Tadessea T, Svoboda MD (2018) Use of remote sensing indicators to assess effects of drought and human induced land degradation on ecosystem health in Northeastern Brazil. Remote Sens Environ 213:129–143. https://doi.org/10.1016/j.rse.2018.04.048
Marques TV, Mendes K, Mutti P, Medeiros S, Silva L, Perez-Marin AM, Campos S, Lúcio PS, Lima K, dos Reis J, Ramos TM, da Silva DF, Oliveira CP, Costa GB, Antonino ACD, Menezes RSC, Santos e Silva CM, Bergson B (2020) Environmental and biophysical controls of evapotranspiration from seasonally dry tropical forests (Caatinga) in the Brazilian Semiarid. Agric For Meteorol 287:107957. https://doi.org/10.1016/j.agrformet.2020.107957
Mata-González R, McLendon T, Martin DW (2005) The inappropriate use of crop transpiration coefficients (Kc) to estimate evapotranspiration in arid ecosystems: a review. Arid Land Res Manag 19:285–295. https://doi.org/10.1080/15324980590951469
Mateos L, González-Dugo MP, Testi L, Villalobos FJ (2013) Monitoring evapotranspiration of irrigated crops using crop coefficients derived from time series of satellite images I. Method validation. Agric Water Manag 125:81–91. https://doi.org/10.1016/j.agwat.2012.11.005
Mu Q, Zhao M, Running SW (2011) Improvements to a MODIS global terrestrial evapotranspiration algorithm. Remote Sens Environ 115:1781–1800. https://doi.org/10.1016/j.rse.2011.02.019
Nagler PL, Glenn EP, Nguyen U, Scott RL, Doody T (2013) Estimating riparian and agricultural actual evapotranspiration by reference evapotranspiration and MODIS enhanced vegetation index. Remote Sens 5:3849–3871. https://doi.org/10.3390/rs5083849
Olivera-Guerra L, Merlin O, Er-Raki S, Khabba S, Escorihuela MJ (2018) Estimating the water budget components of irrigated crops: combining the FAO-56 dual crop coefficient with surface temperature and vegetation index data. Agric Water Manag 208:120–131. https://doi.org/10.1016/j.agwat.2018.06.014
Otkin JA, Martha C, Anderson MC, Hain C, Mladenova IE, Basara JB, Svoboda M (2013) Examining rapid onset drought development using the thermal infrared–based evaporative stress index. J Hydrometeorol 14(4):1057–1074. https://doi.org/10.1175/JHM-D-12-0144.1
Pereira DR, de Mello CR, da Silva AM, Yanagi, SNM (2010) Evapotranspiration and estimation of aerodynamic and stomatal conductance in a fragment of Atlantic Forest in Mantiqueira range region, MG. Cerne 16:32–40. http://repositorio.ufla.br/jspui/handle/1/14209
Peters AJ, Walter-Shea EA, Ji L, Vina A, Hayes M, Svoboda MD (2002) Drought monitoring with NDVI-based standardized vegetation index. Photogramm Eng Remote Sens 68:71–75
Procopio S de O, Cruz MAS, de Almeida MRM, de Jesus Junior LA, Nogueira Junior LR, de Carvalho HWL (2019) SEALBA: região de alto potencial agrícola no Nordeste brasileiro. Aracaju: Embrapa Tabuleiros Costeiros, 2019. (Embrapa Tabuleiros Costeiros, Documentos, 221), p 62
Rampazo NAM, Picoli MCA, de Castro Teixeira AH, Cavaleiro CKN (2020) Water consumption modeling by coupling MODIS images and agrometeorological data for sugarcane crops. Sugar Tech 23:524–535. https://doi.org/10.1007/s12355-020-00919-7
Raupasch MR (2006) Combination theory and equilibrium evaporation. Quart J Roy Meteorol Soc 127:1149–1181. https://doi.org/10.1002/qj.49712757402
Ribeiro MC, Metzger JP, Martensen AC, Ponzoni FJ, Hirota MM (2009) The Brazilian Atlantic Forest: how much is left, and how is the remaining forest distributed? Implications for conservation. Biol Conserv 142:1141–1153. https://doi.org/10.1016/j.biocon.2009.02.021
Safre ALS, Nassar A, Torres-Rua A, Aboutalebi M, Saad JCC, Manzione RL, de Castro Teixeira AH, Prueger JH, McKee LG, Alfieri JG, Hipps LE, Nieto H, White WA, del Mar Alsina M, Sanchez L, Kustas WP, Dokoozlian N, Gao F, Anderson MC (2022) Performance of Sentinel-2 SAFER ET model for daily and seasonal estimation of grapevine water consumption. Irrig Sci 40:635–654. https://doi.org/10.1007/s00271-022-00810-1
Santos MG, Oliveira MT, Figueiredo KV (2014) Caatinga, the Brazilian dry tropical forest: can it tolerate climate changes? Theor Exp Plant Physiol 26:83–99. https://doi.org/10.1007/s40626-014-0008-0
Santos JEO, Cunha FF, Filgueiras R, Silva GH, de Castro Teixeira AH, Silva FCS, Sediyama GC (2020) Performance of SAFER evapotranspiration using missing meteorological data. Agric Water Manag 233:1–8. https://doi.org/10.1016/j.agwat.2020.106076
Seddon AW, Macias-Fauria M, Long PR, Benz D, Willis KJ (2016) Sensitivity of global terrestrial ecosystems to climate variability. Nature 531:229–232. https://doi.org/10.1038/nature16986
Silva COF, de Castro Teixeira AH, Manzione RL (2019) An R package for spatial modelling of energy balance and actual evapotranspiration using satellite images and agrometeorological data. Environ Model Softw 120:104497. https://doi.org/10.1016/j.envsoft.2019.104497
Sun Y, Fu R, Dickinson R, Joiner J, Frankenberg C, Gu L, Xia Y, Fernando N (2015) Drought onset mechanisms revealed by satellite solar-induced chlorophyll fluorescence: Insights from two

contrasting extreme events. J Geophys Res Biogeosci 120:2427–2440. https://doi.org/10.1002/2015JG003150
Teixeira AH de C (2010) Determining regional actual evapotranspiration of irrigated and natural vegetation in the São Francisco River basin (Brazil) using remote sensing and Penman-Monteith equation. Remote Sens 2:1287–1319. https://doi.org/10.3390/rs0251287
Teixeira AH de C, Bastiaanssen WGM, Ahmad MD, Moura MSB, Bos MG (2008) Analysis of energy fluxes and vegetation-atmosphere parameters in irrigated and natural ecosystems of semi-arid Brazil. J Hydrol 362:110–127. https://doi.org/10.1016/j.jhydrol.2008.08.011
Teixeira AH de C, Scherer-Warren M, Hernandez FBT, Andrade RG, Leivas JF (2013) Large-scale water productivity assessments with MODIS Images in a changing Semi-Arid environment: a Brazilian case study. Remote Sens. 5:5783–5804. https://doi.org/10.3390/rs5115783
Teixeira AH de C, Leivas JF, Hernandez FBT, Franco RAM (2017a) Large-scale radiation and energy balances with Landsat 8 images and agrometeorological data in the Brazilian semiarid region. J Appl Remote Sens 11:016030. https://doi.org/10.1117/1.JRS.11.016030
Teixeira AH de C, Leivas JF, Ronquim CC, Silva GB (2017b) The use of MODIS images to quantify the energy balance in different agroecosystems in Brazil. In: Rustamov RB, Hasanova S, Zeylanova MH (eds) Multi-purposeful application of geospatial data. IntechOpen Limited, London, pp 105–121. https://doi.org/10.5772/intechopen.72798
Teixeira AH de C, Leivas JF, Struiving TB, Reis JBRS, Simão FR (2021a) Energy balance and irrigation performance assessments in lemon orchards by applying the SAFER algorithm to Landsat 8 images. Agric. Water Manage. 247:1–9. https://doi.org/10.1016/j.agwat.2020.106725
Teixeira AH de C, Leivas JF, Pacheco EP, Garçon EAM, Takemura CM (2021b) Biophysical characterization and monitoring large-Scale water and vegetation anomalies by remote sensing in the agricultural growing areas of the Brazilian semi-arid region. In: Pandey PC, Sharma LK (eds) Advances in remote sensing for natural resource monitoring. Wiley Online Library, New Jersey, pp 94–109. https://doi.org/10.1002/9781119616016.ch7
Teixeira AH de C, Leivas JF, Takemura CM, Bayma G, Garçon EAM, de Sousa IF, de Farias FJ, Silva COF (2023) Remote sensing environmental indicators for monitoring spatial and temporal dynamics of weather and vegetation conditions: applications for Brazilian biomes. Environ Monit Assess 195:944. https://doi.org/10.21203/rs.3.rs-2573923/v1
Vanella D, Ramírez-Cuesta JM, Intrigliolo DS, Consoli S (2019) Combining electrical resistivity tomography and satellite images for improving evapotranspiration estimates of Citrus orchards. Remote Sens 11(4):373. https://doi.org/10.3390/rs11040373
Venâncio LP, Mantovani EC, do Amaral CH, Neale CMU, Filgueiras R, Gonçalves IZ, da Cunha FF (2021) Evapotranspiration mapping of commercial corn fields in Brazil using SAFER algorithm. Sci Agric 78:1–12. https://doi.org/10.1590/1678-992X-2019-0261
Vicente-Serrano SM, Miralles DG, Domínguez-Castrom F, Azorin-Molina C, El Kenawy A, McVicar TR, Tomás-Burguera M, Beguería S, Maneta M, Peña-Gallardo M (2018) Global assessment of the standardized evapotranspiration deficit index (SEDI) for drought analysis and monitoring. J Climate 31:5371–5393. https://doi.org/10.1175/JCLI-D-17-0775.1
Wolf S, Keenan TF, Fisher JB, Baldocchi DD, Desai AR, Richardson AD, Scott RL, Law BE, Litvak ME, Brunsell NA (2016) Warm spring reduced carbon cycle impact of the 2012 US summer drought. Proc Natl Acad Sci USA 113:5880–5885. https://doi.org/10.1073/pnas.1519620113
Xu X, Liu W, Scanlon BR, Zhang L, Pan M (2013) Local and global factors controlling water-energy balances within the Budyko framework. Geophys Res Lett 40(23):6123–6129. https://doi.org/10.1002/2013GL058324
Yang HB, Qi J, Xu XY, Yang DW, Lv HF (2014) The regional variation in climate elasticity and climate contribution to runoff across China. J Hydrol 517:607–616. https://doi.org/10.1016/j.jhydrol.2014.05.062
Yang Y, Guan H, Batelaan O, McVicar TR, Long D, Piao S, Liang W, Liu B, Jin Z, Simmons CT (2016) Contrasting responses of water use efficiency to drought across global terrestrial ecosystems. Sci Rep 6:1–8. https://doi.org/10.1038/srep23284
Yang Y, Zhang S, Mcvicar TR, Beck HE, Zhang Y, Liy B (2018) Disconnection between trends of atmospheric drying and continental runoff. Water Resour Res 54(7):4700–4713. https://doi.org/10.1029/2018WR022593
Yao Y, Liang S, Qin Q, Wang K (2010) Monitoring drought over the conterminous United States using MODIS and NCEP Reanalysis-2 data. J App Meteorol Climatol 49:1665–1680. https://doi.org/10.1175/2010JAMC2328.1
Zhang X, Zhang B (2019) The responses of natural vegetation dynamics to drought during the growing season across China. J Hydrol 574:706–714. https://doi.org/10.1016/j.jhydrol.2019.04.084
Zhang B, Zhao X, Jin J, Wu P (2015) Development and evaluation of a physically based multiscalar drought index: the Standardized Moisture Anomaly Index. J Geophys Res 120:11575–11588. https://doi.org/10.1002/2015JD023772
Zhang Y, Xiao XM, Zhou S, Ciais P, McCarthy H, Luo YQ (2016) Canopy and physiological controls of GPP during drought and heat wave. Geophys Res Let 43:3325–3333. https://doi.org/10.1002/2016GL068501
Zhang L, Qiao N, Huang C, Wang S (2019) Monitoring drought effects on vegetation productivity using satellite solar-induced chlorophyll fluorescence. Remote Sens 11(378):1–18. https://doi.org/10.3390/rs11040378
Zhang G, Su X, Singh VP, Ayantobo O (2021) Appraising standardized moisture anomaly index (SZI) in drought projection across China under CMIP6 forcing scenarios. J Hydrol: Reg Stud 37:100898. https://doi.org/10.1016/j.ejrh.2021.100898
Zhou L, Zhou G (2009) Measurement and modeling of evapotranspiration over a reed (Phragmitesaustralis) marsh in Northeast China. J Hydrol 372:41–47. https://doi.org/10.1016/j.jhydrol.2009.03.033